



Verification of Electroporation Models Using the Potato Tuber as In Vitro Simulation

José Alvim Berkenbrock^{1,2} · Guilherme Brasil Pintarelli² · Afrânio de Castro Antônio Júnior² · Daniela Ota Hisayasu Suzuki²

Received: 31 August 2017 / Accepted: 23 April 2018 / Published online: 28 April 2018
© Taiwanese Society of Biomedical Engineering 2018

Abstract

Electrochemotherapy (ECT) and Irreversible Electroporation are recent non-thermal techniques employed for the treatment of tumors. These therapies are based on the opening of pores in the cell membrane during application of sufficiently high electric fields. Over the past two decades, clinical trials have validated these therapies in humans. Moreover, ECT has been successfully applied in several species in veterinary clinics. As the therapy depends on the electric field distribution, numerical models and in vitro experiments have an important role in better understanding electric field distribution in biological tissues, especially in anatomically and physiologically complex structures. The potato tuber has emerged as an option for testing the effectiveness of the new electrodes. Potatoes present advantages for several reasons: they are compatible with the 3Rs' concept for animal testing; they are simple to handle; and their electroporated areas become dark after 6–12 h. In this work, we simulated four numerical models from the literature and compared them to in vitro experiments. Our aim was to determine the model that best describes the observable affected area. This is an important point because the models were developed to properly describe tissue variation in electrical conductivity during electroporation, not to determine how electroporation is manifested macroscopically in potato tissue. The area measured with the Miklavčič–Ivorra–Suárez model was in closest agreement to the experiments; however, none of the models exactly represent our in vitro results.

Keywords Electroporabilization · Electrochemotherapy · Non-thermal irreversible electroporation · Vegetal tissue · Numerical model · Pulsed electric field

1 Introduction

Electrochemotherapy (ECT) and Irreversible Electroporation (IRE) for tissue ablation are two recent non-thermal techniques employed for the treatment of tumors [1, 2]. These well-established approaches exploit the physical phenomenon first described as a 'dielectric breakdown', but now called cell electroporation (EP or electroporabilization) [3–6]. From the cell's perspective, during the application of

an electric field (EF) sufficiently high to induce ~1 V transmembrane voltage, the bilayer lipid membrane experiences an electro-mechanical conformation that reduces its normal selectivity [5]. The main theory to explain this increase in conductivity considers the opening of pores around the cell poles, which are resealed after the EF is ceased [7, 8]. This is the same phenomenon behind gene electrotransfer in cell culture [9], DNA vaccines [10], and water treatment for microorganisms [11].

At the tissue level, EP is employed in food processing techniques for conservation [12] and in extraction of macromolecules [13]. As mentioned, new clinical approaches have also been developed based on EP. ECT takes advantage of the transitory pores in the cell membrane to introduce chemotherapy drugs (e.g. bleomycin) into tumor cells [1, 6]. The action of the drugs causes the cells to die. On the other hand, IRE sustains the open pores in order to provoke cell death without additional elements [2, 14].

✉ José Alvim Berkenbrock
j.alvim@usask.ca; eel.jab@gmail.com

¹ Department of Electrical and Computer Engineering, University of Saskatchewan (U of S), Saskatoon, Saskatchewan S7N 5A9, Canada

² Department of Electrical and Electronics Engineering, Institute of Biomedical Engineering, Federal University of Santa Catarina (UFSC), Florianópolis, Santa Catarina 88040-370, Brazil

Over the past two decades, clinical trials have validated these therapies in humans [15, 16]. Moreover, ECT has also been successfully applied in several species in veterinary clinics [17–19]. Notwithstanding this success, as EP is dependent on EF, recent works have shown the need to continue studying EF distribution in biological tissues. Different from treatment of homogeneous tissues, treatment applications close to bones [19] and excitable tissues, such as the heart [20] and brain [21], require attention. Numerical models are a powerful tool that allows scientists, engineers, physicians and veterinarians to better predict EF distribution in anatomically and physiologically complex structures [2, 22, 23].

In 2004, Cima and Mir pointed to the use of the potato tuber as a simple but worthwhile experiment in which conclusions can be extended to animal tissues [24]. Potato tubers present advantages as they are compatible with the concept of the 3Rs in animal testing: reduction of the number of animals, refinement of procedures to reduce distress, and replacement of animal with non-animal techniques) [14, 25]. In vivo confirmation of ECT effectiveness may take weeks by tumor nodule reduction and death. Electroporated zones of potato tissue become dark approximately 6–12 h after the application [14]. Consequently, this simple and relatively rapid technology makes feedback on electroporation effectiveness feasible.

Recent studies have employed potatoes to validate the effectiveness of the size and configuration of new electrodes [26, 27] and to assess the impact of pulse parameters (e.g. frequency and the number of pulses) [28, 29]. This work compares four numerical models found in the literature to in vitro experiments. Our aim is to determine the model that best represents the experimental browned area.

2 Materials and Methods

2.1 In Vitro Preparation

Potatoes (*Solanum tuberosum*) were bought at a local grocery on the day of the experiment, and they were cut into slices 20 mm in thickness and 40 mm in diameter (Fig. 1). The EP protocol was eight pulses with a duration of 100 μs at 1 Hz [1, 22] (Fig. 2). The pulse amplitudes were 210, 270, 330, and 390 V (see Table 1) between two needles 3 mm apart (Fig. 1). The needle depth in the potato was 5 mm; potato thickness does not affect electric field distribution. After the procedure, the potato slices were kept in Petri dishes at room temperature for 24 h. Photographs were taken under constant illumination with a 10 MP, f/2.4, 30 mm, autofocus, Motorola XT1058 (Schaumburg, IL, US) digital camera.

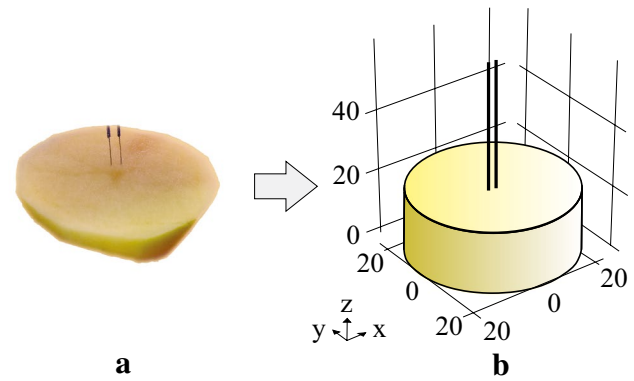


Fig. 1 Needle electrodes inserted into a potato slice, showing a in vitro setup, b in silico geometry

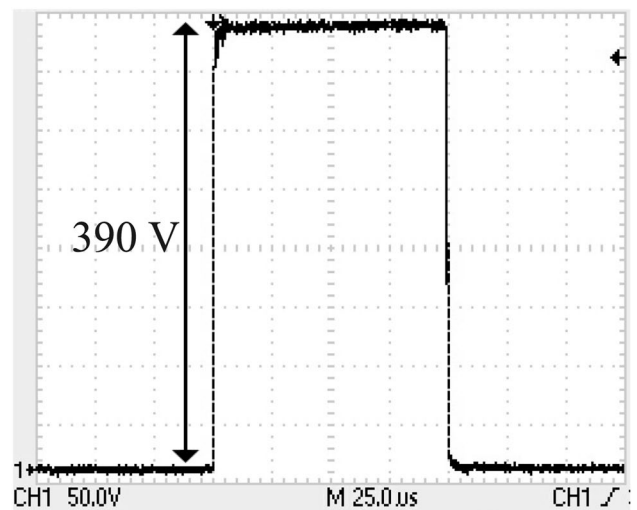


Fig. 2 Applied voltage observed on an oscilloscope. Data acquisition using a Tektronix TDS 2004C (Beaverton, OR, US)

2.2 In Silico Model

The in vitro geometry was simulated by three-dimensional models using COMSOL Multiphysics (COMSOL AB, Sweden). Potato slices 20 mm in height and 40 mm in diameter were built. The two needles were 50 mm in height and 0.6 mm in diameter; they were 3 mm apart. The modeled geometry is presented in Fig. 1. The software automatically generated the fine-grained mesh, resulting in 13,214 tetrahedral elements.

Four models were used to describe the potato tissue behavior. The first considered a constant conductivity ($\sigma=0.03$ S/m [25]). The other three models considered tissue conductivity as a function of the local EF, as follows:

$$\sigma(E) = 0.03 + e^{-e^{-0.01 \cdot (250 - |E|)}} \text{ (S/m)} \tag{1}$$

$$\sigma(E) = 0.15 + 0.6 \cdot e^{-3.153 \cdot e^{-0.00243 \cdot E}} \text{ (S/m)} \tag{2}$$

Table 1 Measured browned areas on potato slices 24 h after electroporation protocol

EF (kV/m)	Voltage (V)	Group I (cm ²)			Group II (cm ²)			Group III (cm ²)			Mean
70	210	0.09	0.06	0.08	0.10	0.13	0.07	0.08	0.11	0.08	0.09
90	270	0.19	0.13	0.08	0.13	0.13	0.07	0.18	0.15	0.20	0.14
110	330	0.13	0.14	0.23	0.34	0.23	0.32	0.31	0.24	0.23	0.24
130	390	0.30	0.14	0.25	0.39	0.33	0.40	0.27	0.30	0.25	0.29

$$\sigma(E) = 0.03 + \frac{0.33}{1 + 10 \cdot e^{\left(\frac{65,000-E}{13,750}\right)}} \text{ (S/m)} \quad (3)$$

Equations (1)–(3) are numerical models for potato tissue conductivity presented by [25, 28, 29] and in this text referred to as Ivorra, Neal, and MIS models, respectively. Calculations were run on a personal computer (Intel Core i5-2500, 3.3 GHz, 4 GB RAM) with a Windows 7 (x64, Microsoft Inc., Redmond, WA, USA) operating system. A steady-state regime was considered, and the applied EFs were 70, 90, 110 and 130 kV/m (See Table 1.) The Dirichlet boundary condition (contact between electrodes and tissue), and Neumann (insulating external surfaces) were applied. The tissue was considered homogeneous, and the Eq. (4) was solved by the finite element method:

$$\nabla \cdot (\sigma \cdot \nabla V) = 0 \quad (4)$$

where σ is the tissue conductivity (S/m) and V is the applied voltage (V).

2.3 Image Processing

The image processing of the in vitro setup was performed using MATLAB (Mathworks, USA). The detection procedure is schematized in Fig. 3. First, the RGB image is converted to grayscale; hence, using a threshold rule, the image is converted into black and white binary. The next step is to detect boundaries and filter images that have a known range of pixels and respect a circle tolerance. This method filters foreign objects. Finally, using a pixel to centimeters' conversion, the area data is displayed in square centimeters (cm²).

The areas from the in silico experiments were measured using the software ImageJ by Color Thresholds.

3 Results

3.1 In Vitro Experiments

Figure 4 presents eight processed images of the 36 samples. The pictures were taken 24 h after EP protocol and processed using the Matlab software. Control experiments showed that the insertion of the needles without EFs does not produce any change [data not presented].

Table 1 shows the values of the area for all samples. In three different days (groups) the EP protocol was applied for the amplitude of different pulses. The mean area by applied EF is presented in the last column.

3.2 In Silico Experiments

The EF distribution in potato tissue for 390 V between electrodes (130 kV/m) is presented in Fig. 5. The models were simulated in 3-D geometries, but only the top potato envelope XY-plane is shown here. The model for constant conductivity ($\sigma = 0.03$ S/m) is presented in Fig. 5a, followed by the models for Ivorra (Fig. 5b), Neal (Fig. 5c), and MIS (Fig. 5d). The color legend on the right indicates EF. Dark red areas have the highest local EF and dark blue means no EF.

4 Discussion

In the last decade, the potato tuber has been increasingly employed to validate new electrodes for medical devices based on EP. Such an approach has been followed for both

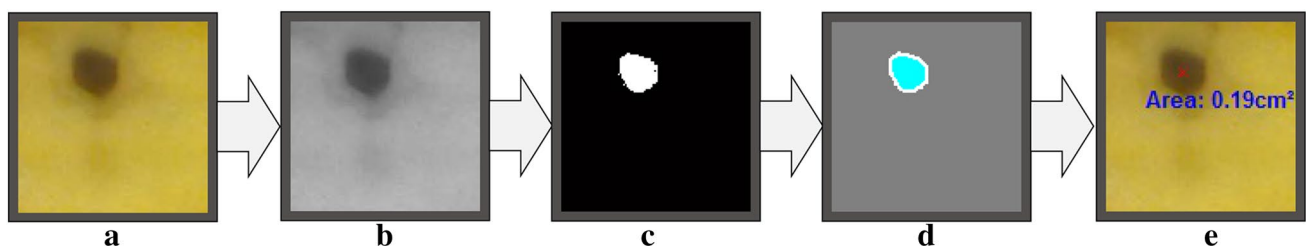


Fig. 3 Image processing software diagram showing **a** Original RGB, **b** grayscale, **c** black and white, **d** circle detection, and **e** area measurement results

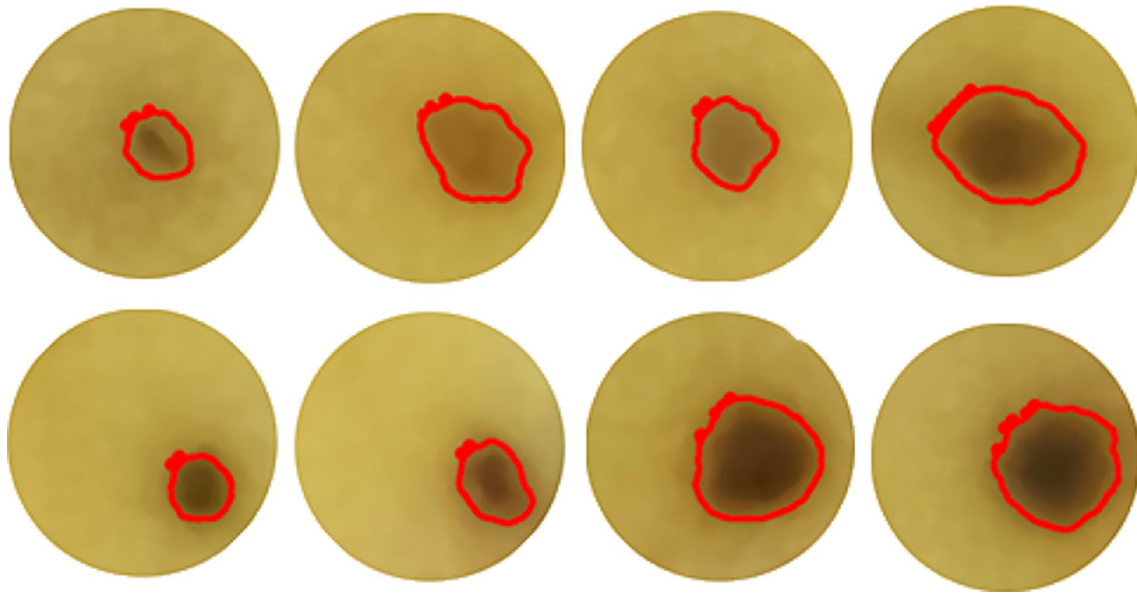


Fig. 4 Browned areas on potatoes 24 h after electroporation protocol (eight pulses of 100 μ s at 1 Hz)

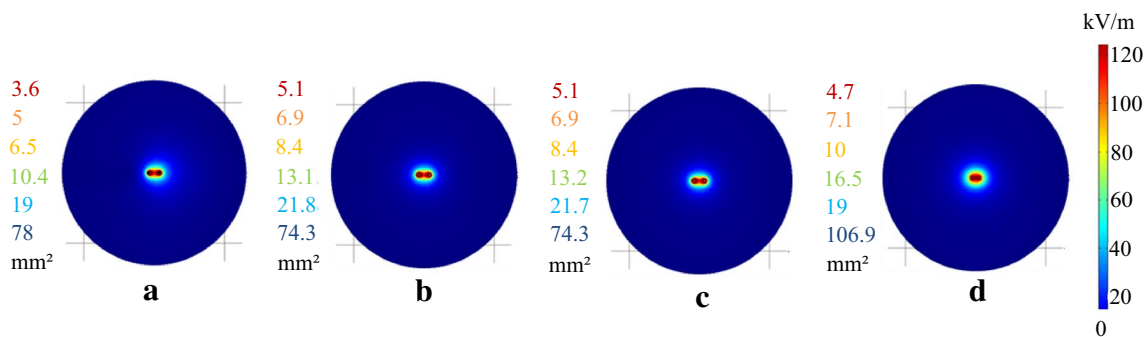


Fig. 5 Simulation of electric field (EF) distribution on potato tissue for 130 kV/m applied. The plane XY was taken from the upper slice surface. As shown by the color legend, dark red is the highest value

of local EF, while dark blue means no EF. **a** Considering constant conductivity, $\sigma=0.03$ S/m, **b** Ivorra model [25], **c** Neal model [28], and **d** MIS model [22, 29]

reversible and irreversible EP-based technologies [21, 26–29]. However, therapy approaches as ECT and IRE impose different requirements on the technology, especially concerning the local EF. A better understanding of EF distribution in biological tissues has been developed through the refinement of numerical models allied to in vitro and in vivo studies [2, 19, 22, 23, 25, 28]. This work used four models from the literature to compare in silico solutions to our in vitro results.

A part of the in vitro results is presented in Fig. 4. The browned area was identified using a Matlab code developed for this purpose. All measurements are presented in Table 1. The average values showed that the browned area increased with the applied EF, which is in agreement with other studies [14, 25, 29].

Four different numerical models were simulated, and the extent of different levels of local EF was measured. The results for a constant conductivity tissue, independent from the local EF, are presented in Fig. 5a. Different models were also considered to describe the tissue conductivity as a function of the EF (Fig. 5b, c, d). The modification of tissue conductivity is a dynamic process, as electroporation changes the amount of cell conductivity, which modifies the surrounding EF distribution. This modification enables other cells to electroporate, similar to a domino effect. The analyzed models specify different conductivity changes. For this reason, a larger difference between models was expected to be observed.

It should be noted that the Ivorra model was especially developed to describe the conductivity of potato tissue

[25], while Miklavcic's model was developed based on rabbit liver tissue and adapted by Suárez for potato tissue [22, 29]. Only the MIS model considered the same EP protocol that was used in our in vitro experiments (i.e., 8 pulses, 100 μ s, 1 Hz). This protocol is used in clinical ECT, despite some variations using 5 kHz [1]. EP effectiveness is influenced by several parameters: the number of pulses, their length, frequency, and amplitude [5, 8]. Considering these influences, the difference between models seen in Fig. 5 might be attributed to the number of pulses applied to the tissue [26, 29].

The browned areas from Table 1 were comparable to the areas in the simulation. Figure 5 presents only the data for 130 kV/m; however, the same methodology was applied to 70, 90, and 110 kV/m [data not presented]. For all experiments, the in vitro browned areas were inside the total extent of EP in silico. The results of this work showed that the numerical models likely predict the extent of the browned areas in the potato after EP protocols. Specifically, we should note that the in vitro means of 29 mm² was closely represented in silico for a local electric field of at approximately 50 kV/m. Ivorra et al. [25] showed that this value of local EF might represent irreversible EP on potato tissue; however, more studies are needed to understand the impact of pulse characteristics and variations.

Potatoes provide a biological tissue model for verification of electroporation effects [14, 24]. This vegetable does not supplant animal use. However, animal experiments may be reduced with new developments of IRE and EQT equipment. The cyan areas in Fig. 5 represent the electric fields above 400 V/cm. This value corresponds to the minimum electric field for successful EQT treatment. 400 V/cm are associated with the browned areas (delimited by the red line) in potatoes (Fig. 4). The browned areas in potatoes are associated with effective EQT treatment.

The potato (*S. tuberosum*) is a consolidated tissue model for electroporation. This work proposed to understand the limitations of the in silico and in vivo models. The electric conductivity of the potato is a model limitation. Potato conductivity is lower than conductivity of normal and tumor tissues. Moreover, potato tissue is more homogeneous than are tumor tissues. Despite the differences, in silico and in vitro (potato) experiments may verify electroporation equipment before applications in the spontaneous tumors of dogs and cats.

At present, we are researching other vegetables with electric conductivity similar to human tissue (about 0.3 S/m), conductivity dependent on the electric field (electroporation effect), and the visual- and short-time verification of effective EQT.

5 Conclusion

The results of this work allowed us to conclude that the tested numerical models may predict the extent of browned areas in potatoes after EP protocols. The MIS model area of 31 mm² was in closest agreement with the 29 mm² observed in vitro. None of the models exactly represent our in vitro results, despite being based on a standardized EP protocol. Potatoes remain as important subjects for 'in vitro simulations' of EP effectiveness, but more studies are necessary to determine the visual reversible/irreversible thresholds.

Acknowledgements The authors thank the Brazilian funding agencies CAPES and CNPq.

Compliance with ethical standards

Conflict of interest The authors declare that they have no conflicts of interest.

Human and animal rights This article does not contain any studies with animal or human participants performed by any of the authors.

References

1. Mir, L. M., Gehl, J., Sersa, G., Collins, C. G., Garbay, J.-R., Billard, V., et al. (2006). Standard operating procedures of the electrochemotherapy: Instructions for the use of bleomycin or cisplatin administered either systemically or locally and electric pulses delivered by the CliniporatorTM by means of invasive or non-invasive electrodes. *European Journal of Cancer Supplements*, 4(11), 14–25. <https://doi.org/10.1016/j.ejcsup.2006.08.003>.
2. Davalos, R. V., Mir, L. M., & Rubinsky, B. (2005). Tissue ablation with irreversible electroporation. *Annals of Biomedical Engineering*, 33(2), 223–231. <https://doi.org/10.1007/s10439-005-8981-8>.
3. Stampfli, R. (1957). Reversible electrical breakdown of the excitable membrane of a Ranvier node. *Anais Academia Brasileira de Ciências*, 30, 57–63. Retrieved from <http://memoria.bn.br/DocReader/158119/11062>. Accessed 23 September 2016.
4. Kinoshita, K., & Tsong, T. Y. (1977). Formation and resealing of pores of controlled sizes in human erythrocyte membrane. *Nature*, 268(5619), 438–441. <https://doi.org/10.1038/268438a0>.
5. Prausnitz, M. R., Bose, V. G., Langer, R., & Weaver, J. C. (1993). Electroporation of mammalian skin: A mechanism to enhance transdermal drug delivery. *Proceedings of the National Academy of Sciences*, 90(22), 10504–10508. <https://doi.org/10.1073/pnas.90.22.10504>.
6. Mir, L. M. (2000). Review article therapeutic perspectives of in vivo cell electropermeabilization. *Bioelectrochemistry*, 53(1), 1–10. [https://doi.org/10.1016/S0302-4598\(00\)00112-4](https://doi.org/10.1016/S0302-4598(00)00112-4).
7. Teissié, J., & Rols, M. P. (1993). An experimental evaluation of the critical potential difference inducing cell membrane electropermeabilization. *Biophysical Journal*, 65(1), 409–413. [https://doi.org/10.1016/S0006-3495\(93\)81052-X](https://doi.org/10.1016/S0006-3495(93)81052-X).
8. Suzuki, D. O. H., Ramos, A., Ribeiro, M. C. M., Cazarolli, L. H., Silva, F. R. M. B., Leite, L. D., et al. (2011). Theoretical and experimental analysis of electroporated membrane conductance in

- cell suspension. *IEEE Transactions on Biomedical Engineering*, 58(121), 3310–3318. <https://doi.org/10.1109/tbme.2010.2103074>.
9. Neumann, E., Schaefer-Ridder, M., Wang, Y., & Hofschneider, P. H. (1982). Gene transfer into mouse lyoma cells by electroporation in high electric fields. *The EMBO Journal*, 1(7), 841–845. <https://doi.org/10.1385/1-59259-409-3:55>.
 10. van Drunen Littel-van den Hurk, S., & Hannaman, D. (2010). Electroporation for DNA immunization: clinical application. *Expert Review of Vaccines*, 9(5), 503–517. <https://doi.org/10.1586/erv.10.42>.
 11. Sarathy, S. R., Sheculski, C., Robinson, J., Walton, J., Soleymani, A., & Kempkes, M. A., et al. (2016). Design, optimization and scale-up of pulsed electric field technologies for large flow applications in heterogeneous matrices (pp. 414–417). https://doi.org/10.1007/978-981-287-817-5_90.
 12. Heinz, V., Alvarez, I., Angersbach, A., & Knorr, D. (2001). Preservation of liquid foods by high intensity pulsed electric fields—basic concepts for process design. *Trends in Food Science & Technology*, 12(3–4), 103–111. [https://doi.org/10.1016/S0924-2244\(01\)00064-4](https://doi.org/10.1016/S0924-2244(01)00064-4).
 13. Kotnik, T., Frey, W., Sack, M., Haberl Meglič, S., Peterka, M., & Miklavčič, D. (2015). Electroporation-based applications in biotechnology. *Trends in Biotechnology*. <https://doi.org/10.1016/j.tibtech.2015.06.002>.
 14. Hjouj, M., & Rubinsky, B. (2010). Magnetic resonance imaging characteristics of nonthermal irreversible electroporation in vegetable tissue. *The Journal of Membrane Biology*, 236(1), 137–146. <https://doi.org/10.1007/s00232-010-9281-2>.
 15. Matthiessen, L. W., Johannesen, H. H., Hendel, H. W., Moss, T., Kamby, C., & Gehl, J. (2012). Electrochemotherapy for large cutaneous recurrence of breast cancer: A phase II clinical trial. *Acta Oncologica*, 51(6), 713–721. <https://doi.org/10.3109/0284186X.2012.685524>.
 16. Mali, B., Jarm, T., Snoj, M., Sersa, G., & Miklavcic, D. (2013). Antitumor effectiveness of electrochemotherapy: A systematic review and meta-analysis. *European Journal of Surgical Oncology: The Journal of the European Society of Surgical Oncology and the British Association of Surgical Oncology*, 39(1), 4–16. <https://doi.org/10.1016/j.ejso.2012.08.016>.
 17. Cemazar, M., Tamzali, Y., Sersa, G., Tozon, N., Mir, L. M., Miklavcic, D., et al. (2008). Electrochemotherapy in veterinary oncology. *Journal of Veterinary Internal Medicine*, 22(4), 826–831. <https://doi.org/10.1111/j.1939-1676.2008.0117.x>.
 18. Spugnini, E. P., Renaud, S. M., Buglioni, S., Carocci, F., Dragonetti, E., Murace, R., et al. (2011). Electrochemotherapy with cisplatin enhances local control after surgical ablation of fibrosarcoma in cats: An approach to improve the therapeutic index of highly toxic chemotherapy drugs. *Journal of Translational Medicine*, 9(1), 152. <https://doi.org/10.1186/1479-5876-9-152>.
 19. Suzuki, D. O. H., Berkenbrock, J. A., de Oliveira, K. D., Freytag, J. O., & Rangel, M. M. M. (2016). Novel application for electrochemotherapy: Immersion of nasal cavity in dog. *Artificial Organs*. <https://doi.org/10.1111/aor.12858>.
 20. Deodhar, A., Dickfeld, T., Single, G. W., Hamilton, W. C., Thornton, R. H., Sofocleous, C. T., et al. (2011). Irreversible electroporation near the heart: Ventricular arrhythmias can be prevented with ECG synchronization. *American Journal of Roentgenology*, 196(3), W330–W335. <https://doi.org/10.2214/AJR.10.4490>.
 21. Bonakdar, M., Wasson, E. M., Lee, Y. W., & Davalos, R. V. (2016). Electroporation of brain endothelial cells on chip toward permeabilizing the blood-brain barrier. *Biophysical Journal*, 110(2), 503–513. <https://doi.org/10.1016/j.bpj.2015.11.3517>.
 22. Miklavcic, D., Sel, D., Cukjati, D., Batiuskaite, D., Slivnik, T., & Mir, L. M. (2004). Sequential finite element model of tissue electroporation. In Conference proceedings: Annual international conference of the IEEE Engineering in Medicine and Biology Society. IEEE Engineering in Medicine and Biology Society. Annual Conference, Vol. 5, No. 5, pp. 3551–3554. <https://doi.org/10.1109/ieems.2004.1403998>.
 23. Ramos, A. (2005). Effect of the electroporation in the field calculation in biological tissues. *Artificial Organs*, 29(6), 510–513. <https://doi.org/10.1111/j.1525-1594.2005.29085.x>.
 24. Cima, L. F., & Mir, L. M. (2004). Macroscopic characterization of cell electroporation in biological tissue based on electrical measurements. *Applied Physics Letters*, 85(19), 4520. <https://doi.org/10.1063/1.1818728>.
 25. Ivorra, A., Mir, L. M., & Rubinsky, B. (2009). Electric field redistribution due to conductivity changes during tissue electroporation: Experiments with a simple vegetal model. In IFMBE Proceedings, Vol. 25, No. 13, pp. 59–62. <https://doi.org/10.1007/978-3-642-03895-2-18>.
 26. Bonakdar, M., Latouche, E. L., Mahajan, R. L., & Davalos, R. V. (2015). The feasibility of a smart surgical probe for verification of IRE treatments using electrical impedance spectroscopy. *IEEE Transactions on Biomedical Engineering*, 62(11), 2674–2684. <https://doi.org/10.1109/TBME.2015.2441636>.
 27. Campana, L. G., Dughiero, F., Forzan, M., Rossi, C. R., & Sieni, E. (2016). A prototype of a flexible grid electrode to treat widespread superficial tumors by means of Electrochemotherapy. *Radiology and Oncology*, 50(1), 49–57. <https://doi.org/10.1515/raon-2016-0013>.
 28. Neal, R. E., Garcia, P. A., Robertson, J. L., & Davalos, R. V. (2012). Experimental characterization and numerical modeling of tissue electrical conductivity during pulsed electric fields for irreversible electroporation treatment planning. *IEEE Transactions on Biomedical Engineering*, 59(4), 1076–1085. <https://doi.org/10.1109/TBME.2012.2182994>.
 29. Suárez, C., Soba, A., Maglietti, F., Olaiz, N., & Marshall, G. (2014). The role of additional pulses in electroporation protocols. *PLoS ONE*, 9(12), e113413. <https://doi.org/10.1371/journal.pone.0113413>.